Research Square

Preprints are preliminary reports that have not undergone peer review.
They should not be considered conclusive, used to inform clinical practice,
or referenced by the media as validated information.

Spatiotemporal Ferro-Ionic Dynamics in Van der Waals Ferroelectrics

Weiyou Yang

weiyouyang@tsinghua.org.cn

Institute of Micro/Nano Materials and Devices, Ningbo University of Technology
https://orcid.org/0000-0002-3607-3514

Muzhi Li

Changsha University of Science & Technology

Xingan Jiang

Institute of Micro/Nano Materials and Devices, Ningbo University of Technology
https://orcid.org/0000-0001-9680-756X

Zhuoyin Peng

Changsha University of Science & Technology

Dongdong Zhang

Ningbo University of Technology https://orcid.org/0000-0002-0091-1803

Xue Chen

Chinese Academy of Sciences

Xiangping Zhang

Department of Materials Science and Engineering, Southern University of Science and Technology

Xueyun Wang

School of Aerospace Engineering & State Key Laboratory of Environment Characteristics and Effects for Near-space, Beijing Institute of Technology https://orcid.org/0000-0001-5264-9539

Zhao Liang

Ningbo University of Technology https://orcid.org/0000-0003-3524-4761

Article

Keywords:

Posted Date: April 2nd, 2026

DOI: https://doi.org/10.21203/rs.3.rs-9253312/v1

License: This work is licensed under a Creative Commons Attribution 4.0 International License.
Read Full License

Additional Declarations: There is **NO** Competing Interest.

Spatiotemporal Ferro-Ionic Dynamics in Van der Waals Ferroelectrics

Muzhi Li[1, 2], Xingan Jiang[1, *], Zhuoyin Peng[2], Dongdong Zhang[1], Xue Chen[3], Xiangping Zhang[4], Xueyun Wang[5], Zhao Liang[1, *] and Weiyou Yang[1, *]

[1]*Institute of Micro/Nano Materials and Devices, Ningbo University of Technology, Ningbo, 315211, China*

[2]*School of Energy and Power Engineering, Changsha University of Science & Technology, Changsha, 410014, P. R. China.*

[3]*Engineering Research Center for Semiconductor Integrated Technology, Institute of Semiconductors, Chinese Academy of Sciences, Beijing, 100083, China.*

[4]*Department of Materials Science and Engineering, Southern University of Science and Technology, Shenzhen, Guangdong, China.*

[5]*School of Aerospace Engineering, Beijing Institute of Technology, Beijing, 100081, China.*

[*]Corresponding author: Xingan Jiang; Zhao Liang; Weiyou Yang

Email: Jiangxa88@163.com, walleliang@hnu.edu.cn and weiyouyang@tsinghua.org.cn.

Van der Waals $CuInP_2S_6$ represents a model ferro–ionic system where copper ion migration controls the polarization states and current evolution, having exciting applications in neuromorphic computing and memristive devices. However, a fundamental challenge still remains in resolving the long-standing uncertainty about the origin of dynamic currents in ferroionic system. Herein, based on a pulsed tip-based methodology, the present work accomplishes efficient manipulation of nanoscale ferro-ionic dynamics and disentangles the individual contribution from ferroelectric switching to dynamic currents. Moreover, this work further reveals the origin of multiple current peaks and establishes a mechanism of spatiotemporal ferro-ionic dynamics. This mechanistic insight goes beyond previous studies that focused solely on temporal or electric-field dependence, which is an important step toward high-performance ferroionic memristors.

Rapid development of artificial intelligence demands advanced computing technologies to overcome the von Neumann bottleneck[1-3]. Low dimensional ferroelectrics have thus sparked intensive interest for memristors and neuromorphic computing in miniaturized device[4-9]. Such interest is further fueled by ferro-ionic coupling — the inherent coupling of switchable polarization with ionic migration — which provides new degrees of freedom for manipulating memristive behaviors[10-14].

Van der Waals (vdW) $CuInP_2S_6$ (CIPS) is a model system with remarkable ferro-ionic properties[15-20]. Under an electric field, the Cu ions migrate within or across vdW layers, thus controlling the polarization along or against electric field. This coupling process also generates a dynamic current response, which is the fundamental for cutting-edge applications such as memristors[21-27]. Recent years have witnessed the significant progress. For instance, Jiang *et al.* investigated the polarization dynamics and current modulation in CIPS via indirect SS-PFM technique[28]; Liang *et al.* reported the polarization kinetics-controlled photovoltaic behaviors[29]. However, some critical questions still remain in this material system. Specifically, how the nanoscale ferroelectric domain dynamics influence the current under *dc* electric field, and how to disentangle their contributions to the current response, are crucial for comprehensive mechanistic understanding.

Herein, this work achieves the efficient manipulation of the spatiotemporal ferro-ionic dynamics and resolves the long-standing ambiguity in current source within ferro-ionic systems. By in-situ tracking of nanoscale polarization dynamics, this work disentangles the individual contribution from ferroelectric switching to current evolution. Furthermore, this work unveils the tunable current peaks and demonstrates its origin based on the spatiotemporal domain dynamics. Our work bridges the gap between spatiotemporal ferro–ionic dynamics and current control, providing a critical understanding for the design of high performance ferroionic memristors.

Results

Spatiotemporal ferroelectric domain dynamics under biased tip

The ferroelectricity primarily arises from Cu^+ ions occupying different sites (Fig. 1a)[30,31], which can be manipulated by electric[15,16], mechanical[32,33], and optical field[34]. The Cu ions migrate to the upper/lower sites within the layer, thus exhibiting upward/downward polarization state ($\boldsymbol{P}\uparrow/\boldsymbol{P}\downarrow$),

respectively. Prior reports[15, 24, 25, 27, 28, 35-38] indicated that the intralayer Cu migration exhibited a lower energy barrier (~0.23-0.7 eV) than interlayer migration across vdW gaps (~0.6-1.58 eV), which could be overcome by external fields. For instance, under lower electric field (***E***↓) (Fig. 1b), the Cu ions migrate to the lower site and switch the polarization from ***P***↑ to ***P***↓ (***E***↓***P***↓). However, under a higher field or prolonged time, the Cu ions migrate across vdW gap to adjacent layer, switching the polarization to ***P***↑ opposed to the field (***E***↓***P***↑). The Cu ion migration and its directionality under electric fields were also experimentally verified by the reports[39, 40].

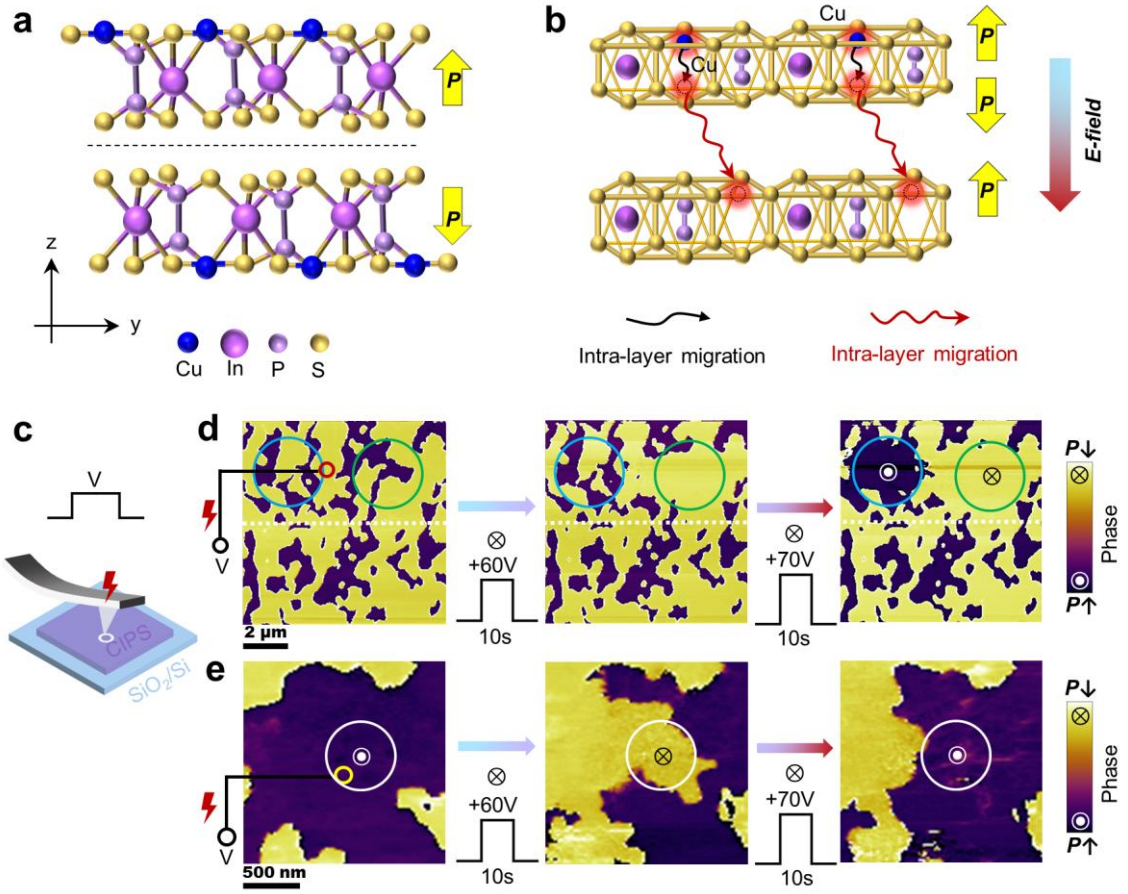


Fig. 1 | Spatiotemporal polarization switching via controlled Cu ionic migration pathways. a Two stable polarization states (***P***↑/***P***↓) from different Cu ion occupations. **b** Schematic of polarization switching pathways. **c** Schematic of tip voltage applied at a point location with an open-circuit condition. **d** Domain switching under tip voltage. Significant switching occurs near the tip, in contrast to the remote regions (below the white dashed line). **e** Tip voltage induced cyclic switching of ***P***↑→***P***↓→***P***↑.

Figs. 1c, d verify the spatiotemporal ferroelectric domain dynamics visualized by piezoresponse force microscopy (PFM) technique[41]. In our experiments, high-quality crystals with a typical stoichiometric ratio of ~1:1:2:6 (Supplementary Fig. 1) is grown and mechanically exfoliated to ~90 nm-thick nanosheets on substrates. An insulating SiO_2/Si substrate is utilized to form an open-circuit condition, and the voltage is applied via the conductive tip (Fig. 1c). The open-circuit setup can

withstand high voltage without generating currents. For example, even after consecutive application of +60 V and +70 V bias (10 s each), the sample also shows minimal surface damage (with a height change of ~1-4 nm beneath tip) while achieving substantial domain control over microscale distance (Supplementary Fig. 2).

A shown in Fig. 1d, the purple-black and yellow regions corresponds to the polarization pointing upward (***P***↑) and downward (***P***↓), respectively (Supplementary Fig. 3). Interestingly, on both sides of tip position, the blue and green circled regions show significant domain switching in opposite directions. After applying +60 V and +70 V for 10 s each, the purple-black domains (***P***↑) in the green circled region are eventually switched to yellow domains (***P***↓), aligning with the tip field (***E***↓***P***↓) due to Cu ions intralayer migration[15,16]. In the blue circled region, yellow domains (***P***↓) are eventually switched to purple-black domains (***P***↑), with the opposite direction to the tip field (***E***↓***P***↑) due to Cu ions interlayer migration[42]. The switching difference in spatial regions near the tip is highly reproducible (Supplementary Fig. 4), which is attributed to the non-uniform tip electric field from the asymmetry geometry or the tilt of AFM tip (Supplementary Fig. 5). Furthermore, Fig. 1e and Supplementary Fig. 6 show the cyclic switching of ***P***↑ → ***P***↓ → ***P***↑, which can be interpreted as quantized charge transport by sequential Cu ion migration across vdW gap[43]. Additionally, the switching spectroscopy PFM technique[16] also confirms the cyclic switching behaviors (Supplementary Fig. 7).

The dynamic current response during ferroelectric switching process

Next, we turn our attention to in-situ tracking of the ferroelectric dynamics and current response under a biased tip. As shown in Fig. 2a, the tip position is marked by the white circle, the voltage is applied via the conductive substrate (Au/SiO_2/Si). The results show the remarkable domain evolution near the tip after five pulses (+8V/3s), where the pristine domains are marked by the blue outline. The domain change is defined as $\Delta D_n = D_n - D_0$ (D_0 and D_n refer to the pristine domain and that after n^{th} pulse, respectively). Fig. 2b shows the bidirectional domain switching after the 1st pulse, where the yellow domains (***P***↓) are switched back to purple-black domains (***P***↑), as indicated by the white arrow. Meanwhile, the purple-black domains (***P***↑) are switched to the yellow domains (***P***↓), as indicated by the yellow arrow. With 2nd to 5th pulses, the switched regions are progressively expanded. However, in the yellow arrow-marked area, the area of yellow domains (***P***↓) changes alternatively by: increasing

from D_0 to D_3, decreasing from D_3 to D_4, and increasing again from D_4 to D_5. The magnified views before/after 1-5th pulses (Supplementary Fig. 8) reveal the successive switching $\boldsymbol{P}\uparrow \rightarrow \boldsymbol{P}\downarrow \rightarrow \boldsymbol{P}\uparrow \rightarrow \boldsymbol{P}\downarrow$, including two complete cycles of $\boldsymbol{P}\uparrow \rightarrow \boldsymbol{P}\downarrow \rightarrow \boldsymbol{P}\uparrow$ and $\boldsymbol{P}\downarrow \rightarrow \boldsymbol{P}\uparrow \rightarrow \boldsymbol{P}\downarrow$.

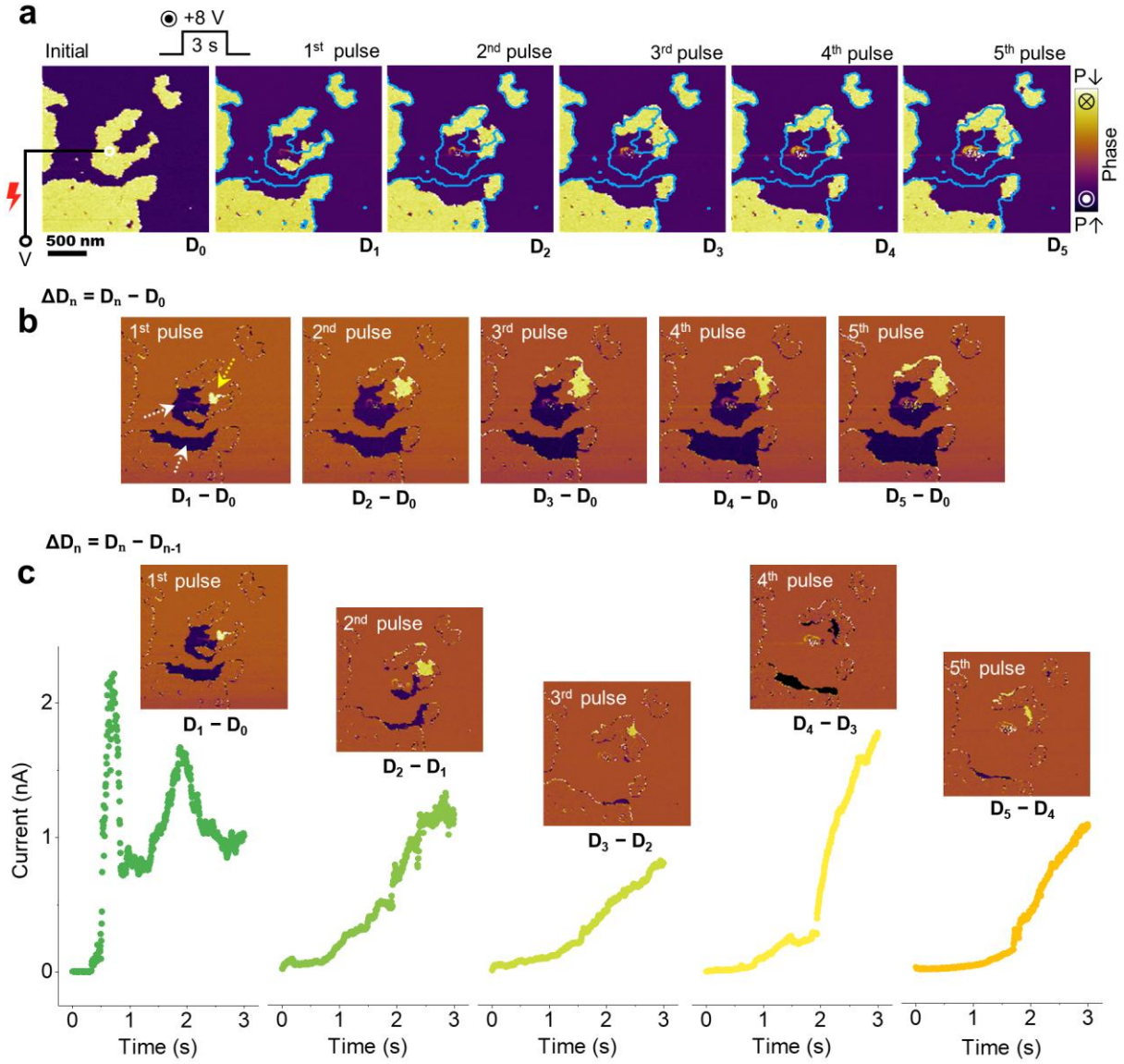


Fig. 2 | Polarization switching and current response under a biased tip. a Domain evolution after five pulses (+8V/3s) using tip voltage. The pristine domain is labeled as D_0, the domain after the nth pulse is denoted as D_n. **b** The switched domain extracted from panel **a** after five pulses according to $\Delta D_n = D_n - D_0$. **c** The measured *I-t* response during each pulse and the switched domain extracted from panel **a** according to $\Delta D_n = D_n - D_{n-1}$.

The switched domains by nth pulse are defined as $\Delta D_n = D_n - D_{n-1}$ (D_{n-1} denotes the domain after (n-1)th pulse). The current response and switched domains after each pulse are provided in Fig. 2c. It seems that the measured currents with AFM tip are sensitive to the tip conditions, however it does not compromise the strong relation between domain dynamics and current responses. It implies that

the current magnitude relates to switched domain area, namely, larger switched area yields higher current. Correspondingly, the most remarkable domain changes during the 1st pulse coincide with the maximal current, and the two current peaks correspond to two distinct domain switching events. Supplementary Fig. 9 presents the quantified domain area and maximum current for each pulse, also demonstrating the clear scaling between switched domain areas and current values.

Disentangling the contribution from ferroelectric switching to currents

To unveil the origin of current behavior, the varied pulse conditions were applied at distinct locations. Four sets of pulses are applied on purple-black ($\boldsymbol{P}\uparrow$) and yellow domains ($\boldsymbol{P}\downarrow$) (Fig. 3a and Supplementary Fig. 10), and the tip positions are marked by blue and red circles. The pulse width (t_{pw}) is fixed at 0.1 s, with gradual increase in pulse voltages. During the 2nd set (V_{max} = 5 V), the currents at both locations begin to increase significantly with the bias voltage, yet without domain change. These results indicate that the polarization direction is not the primary cause of notable current increase. Meanwhile, the current difference between both locations is also tiny, further verifying the minimal influence of polarization orientation related to interface barriers at the tip-sample contact[44]. During the 3th set (V_{max} = 7 V), the domain switching emerges near position 1 (white frame), while the domains near position 2 remain unchanged. Correspondingly, the current difference between both locations becomes pronounced, with much higher currents at position 1 than that at position 2. These experimental results confirm that the remarkable current difference between two locations principally arises from the polarization switching current. However, during the 4th set (V_{max} = 10 V), significant domains switching occurs at both locations. In such case, the current surges at both locations beyond the detection limit (20 nA), once exceeding a threshold voltage of ~ 8 V.

Fig. 3b and Supplementary Fig. 11 further disentangle the contribution from ferroelectric switching to dynamic current. During 1st voltage set, the domain changes occur near tip position, where the yellow domains ($\boldsymbol{P}\downarrow$) are switched to purple-black ones ($\boldsymbol{P}\uparrow$) (white frame). As domain switching areas are close at two different locations, the current magnitude and its evolution are strikingly identical, indicating the reliable and reproducible results (Supplementary Fig. 12). During 2nd voltage set, no domain changes are observed, which rules out that the measured current (red line) arises from domain switching. Instead, it indicates that the gradually increased current over time (red line) is mainly attributable to Cu ion migration or other leakage current. Thus, the contribution from

domain switching to the current can be effectively disentangled by the current difference between two voltage sets, featuring a well-separated current peak for domain switching current.

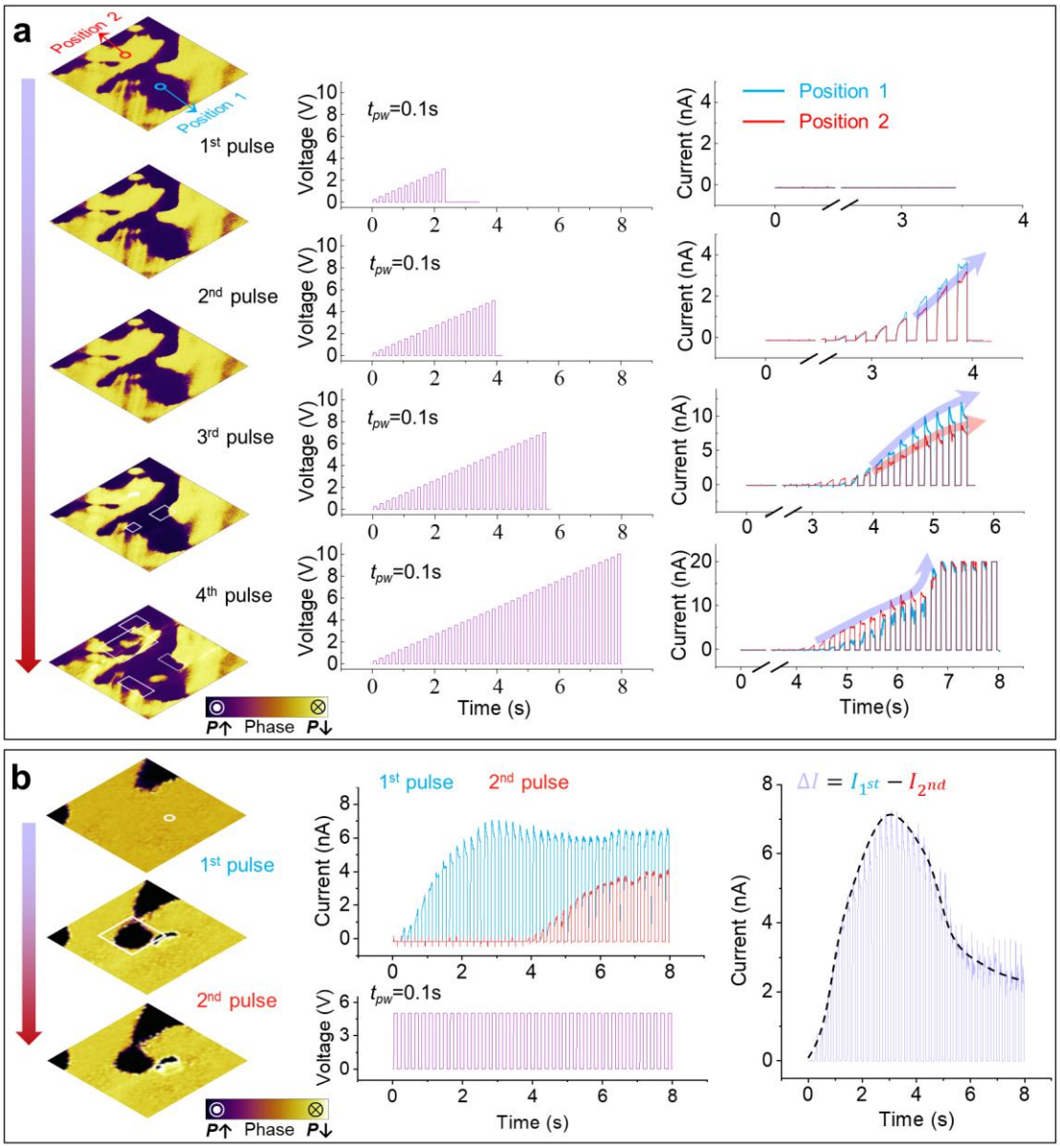


Fig. 3 | Disentangling the contributions from ferroelectric switching dynamics to currents. a Simultaneous tracking of domain changes and current response under four sets of voltage pulses applied to two different domain regions. The region is 850 nm×850 nm. **b** Simultaneous tracking of domain changes and current response under two sets of pulses. The tip position is marked by white circle. The region is 335 nm×335 nm.

Highly tunable current peaks by varying the pulse voltage

The tunability of current peaks was verified by varying the electric pulse parameters such as amplitude, duration, and repetition, which can be attributed to the intrinsically slow kinetics of ion migration[45,46]. As shown in Fig. 4a, three sets of voltage pulses are applied at different locations,

with the pulse voltages and numbers fixed at 5 V and 25 cycles, respectively, by increasing the pulse width (t_{pw}) from 0.01 to 0.1, and finally to 1 s. At a short pulse width (t_{pw} =0.01 s), the current increases monotonically with the increase of pulse numbers. As the t_{pw} increases to 0.1 or 1s, one or two current pearks emerges. Notably, such pulse width-controlled current peaks are highly reproducible across random locations (Supplementary Fig. 13). Similarly, 15 cycles of bipolar triangular wave voltage (V_{max} =±8 V) are further applied, resulting in the emergence of multiple current peaks (Fig. 4b), and the corresponding *I-V* curves are provided in Fig. 4c. The existence of remarkable current rectification could be mainly attributed to the Cu ion accumulation/depletion beneath the tip under positive/negative voltages[21,47].

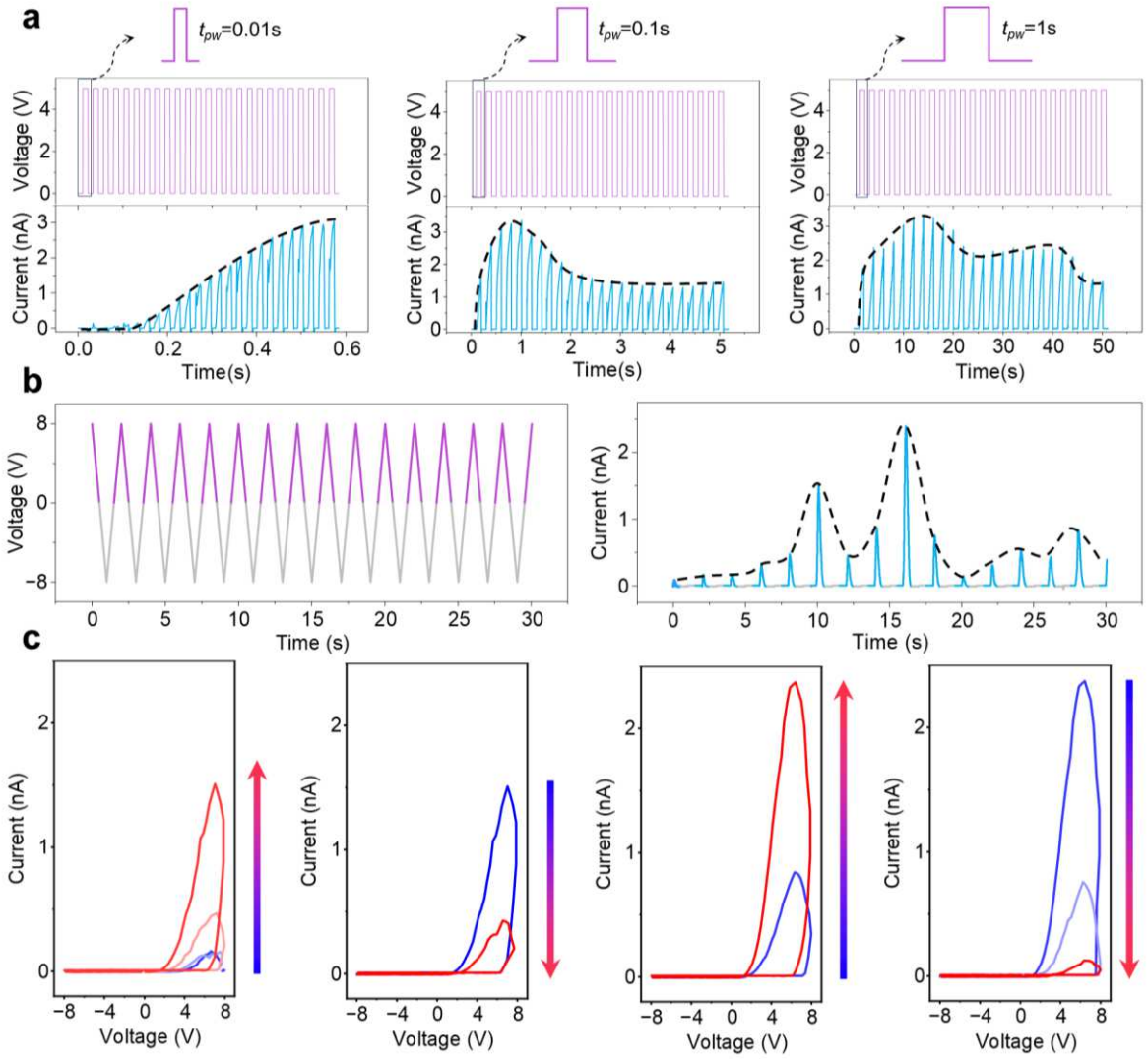


Fig. 4 | Highly controllable current modulation via varying pulse voltage. a Current response under varied pulse width (t_{pw}). Pulse width varies from 0.01 s to 0.1 s and finally to 1 s. **b** Current response measured under triangular wave stimulation (±8 V, 15 cycles). **c** The corresponding the *I-V* curves measured under triangular wave bias stimulation.

Unraveling the origin of multiple current peaks

Furthermore, the nanoscale origin of tip-collected multiple current peaks was unveiled by spatiotemporal domain dynamics, as shown in Fig. 5. It is worth noting that the AFM tip has a typically asymmetric geometry (Supplementary Fig. 2), thus generating a spatially non-uniform electric field. Moreover, during voltage application, the AFM tip is subjected to complex localized forces (*e.g.*, electrostatic forces, electromechanical coupling), which can apply complex torques to tilt the tip in any arbitrary direction. As a result, the tip electric field tilts in accordance with the tip inclination (Fig. 5a), which can be confirmed by the spatiotemporal domain dynamics. It discloses that the domain-switching regions are highly correlated with the spatial distribution of tilted tip electric fields (Fig. 5b). During the 1st voltage set, two current peaks (I_1 and I_2) appear in the *I-t* curve. Correspondingly, the ferroelectric domain switching occurs within two distinct regions (Region #1 and #2). The current peaks I_1 and I_2 originate from the tip-collected currents generated in Region #1 and Region #2, respectively. Specifically, Region #1 locates in the area closer to the tip, where the domain switching area and the tip collected current are larger, due to the stronger electric field intensity. Region #2 locates in the annular area far away from the tip, where the domain switching area and the tip-collected current are smaller, due to the weaker electric field intensity and annular distribution of tip electric field. As the 2nd pulse is further applied, the domain switching primarily occurs within the area closer to the tip (Region #1), resulting in the generation of one current peak. Therefore, these experimental observations unveil the origin of multiple current peaks.

These key phenomena as revealed above are highly reproducible across random locations (Supplementary Figs.14, 15), validating the mechanism that spatiotemporal domain dynamics control the emergency and evolution of current peaks. Figs. 5c, d depict the scenario of Cu ions migration and tip-collected current under tip electric field. It discloses that the multiple current peaks arise from the domain switching occurring within distinct spatial regions near the tip. Moreover, the present tip-based approach can locally collect the currents from distinct regions near the tip, showing the capacity and advantage to disentangle the contributions from domain switching dynamics to dynamic currents.

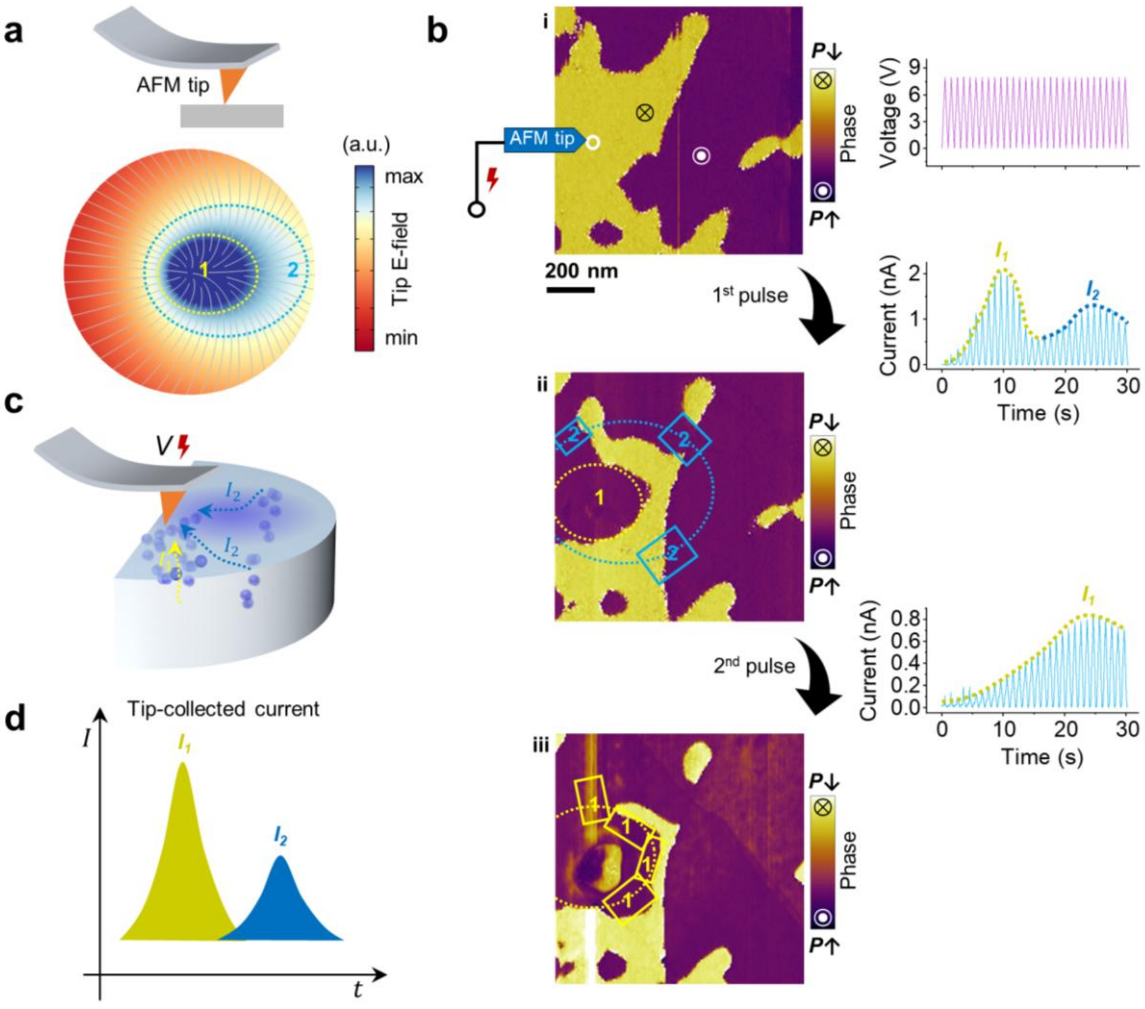


Fig. 5 | Origin of tip-collected multiple current peaks. a The simulated tip electric field distribution. Tip asymmetry or tilting deviates the field from a symmetric radial distribution. **b** The as-measured ferroelectric domain changes and corresponding current response under two sets of 30 cycles of triangular wave bias (± 8 V_{max}). **c** The scenario of Cu ions migration and tip-collected current under tip electric field. **d** Schematic of corresponding tip-collected current peaks.

Discussion

In summary, this work demonstrates the dynamic current manipulation driven by spatiotemporal ferro-ionic dynamics in the van der Waals ferroionic system $CuInP_2S_6$. Using a pulsed tip-voltage methodology, we achieve efficient control of ferroelectric dynamics and directly correlate their spatiotemporal dynamics with current evolution. This work successfully disentangles the individual contribution of nanoscale ferroelectric switching to the dynamic current. Furthermore, this work unveils the tunable current peaks, and clarify its nanoscale origin through establishing a mechanism of spatiotemporal ferro-ionic dynamics. Our findings resolve the long-standing uncertainty about the

origin of current source in ferroionic system, which is a key step toward high-performance ferroionic memristors.

Methods

Materials and Methods

Crystal growth and material preparation

CIPS single crystals are grown via chemical vapor transport[28]. Stoichiometric amounts of elemental precursors are sealed in a quartz tube under a vacuum of approximately 10^{-3} Pa. The tube is then placed in a two-zone furnace, where the hot and cold zones are maintained at temperatures of ~665 °C and ~610 °C, respectively. After ~212 hours of reaction time, the as-grown CIPS crystals are mechanically exfoliated using adhesive tape to obtain thin flakes. These flakes are then transferred onto Au-coated silicon substrates for further characterization, including piezoresponse force microscopy (PFM), switching spectroscopy PFM (SS-PFM), and conductive atomic force microscopy (c-AFM) measurements.

Atomic force microscopy measurement

The piezoresponse force microscopy (PFM) measurements are conducted on thin flakes using a commercial atomic force microscope (Cypher S, Oxford Instruments, USA) equipped with a high-voltage module. The ferroelectric domains are imaged in PFM mode with a Pt/Ir-coated Si cantilever tip driven by an AC voltage (V_{AC} = 1-3 V) at ~340-360 kHz. Switching spectroscopy PFM (SS-PFM) is employed to measure polarization hysteresis loops. In c-AFM measurements, the voltage is applied through the sample's bottom electrode and the nanometer tip collects the currents.

Simulation of tip-electric field distribution

The electric field distribution between the tip-sample was modeled using the finite element method. The CIPS nanosheet was represented as a cylinder, surrounded by a spherical air domain. Relative dielectric constants of 1 and 40 were assigned to air and CIPS, respectively. Simulations were performed with the AC/DC Module, where electrical boundary conditions were defined: the bottom surface of the CIPS was grounded, representing the boundary potential at infinity of the spherical air domain, while a preset voltage was applied to the tip surface. The field distribution was computed via

a stationary study.

Data availability

All data supporting the findings of this study are available within the article and the Supplementary Information file.

References

[1] Sharma, D. et al. Linear symmetric self-selecting 14-bit kinetic molecular memristors. *Nature* **633**, 560 (2024).

[2] Pei, J. et al. Towards artificial general intelligence with hybrid Tianjic chip architecture. *Nature* **572**, 106-111 (2019).

[3] Yan, A. et al. A flexible digital compute-in-memory chip for edge intelligence. *Nature* 649, 1165 (2026).

[4] Wu, G. et al. Ferroelectric-defined reconfigurable homojunctions for in-memory sensing and computing. *Nat. Mater.* **22**, 1499 (2023).

[5] Li, E. et al. Ferroelectric Transistors: from Materials Innovation to Intelligent Electronic Systems. *Adv. Mater*. **e15480** (2025)

[6] Bian, R. *et al.* Developing fatigue-resistant ferroelectrics using interlayer sliding switching. *Science* **385**, 57-62(2024).

[7] He, R. et al. Switching Two-Dimensional Sliding Ferroelectrics by Mechanical Bending. *Phys. Rev. Lett.* **134**, 076001 (2025).

[8] Luo, C. et al. Opto-Ferroelectric Coupling Enhanced α-In_2Se_3 Transistors With Light-Controlled Mode Switchover. *Adv Mater.* **38**, e14329 (2026).

[9] Wu, J. et al. High tunnelling electroresistance in a ferroelectric van der Waals heterojunction via giant barrier height modulation. *Nat. Electron*. **3**, 1 (2020).

[10] Wang, X. et al. Electrical and magnetic anisotropies in van der Waals multiferroic $CuCrP_2S_6$. *Nat. Commun.* **14**, 840 (2023).

[11] Ma, Y. et al. High-performance van der Waals antiferroelectric $CuCrP_2S_6$-based memristors. *Nat. Commun.* **14**, 7891 (2023).

[12] Xu, X. et al. Multifunctionality of $Li_2SrNb_2O_7$: memristivity, tunable rectification, ferroelasticity, and ferroelectricity. *Adv. Mater.* **34**, 2206022 (2022).

[13] Wang, C. et al. Towards two-dimensional van der Waals ferroelectrics. *Nat. Mater.* **22**, 542 (2023).

[14] Zhang, D. et al. Ferroelectric order in van der Waals layered materials. *Nat. Rev. Mater*. **8**, 25–40 (2023).

[15] Neumayer, S. et al. Alignment of polarization against an electric field in van der Waals ferroelectrics. *Phys. Rev. Appl.* **13**, 064063 (2020).

[16] Li, T. et al. Realization of sextuple polarization states and interstate switching in antiferroelectric $CuInP_2S_6$. *Nat. Commun.* **15**, 2653 (2024).
[17] Brehm, J. A. et al. Tunable quadruple-well ferroelectric van der Waals crystals. *Nat. Mater*. **19**, 43–48 (2020).
[18] Wang, K. et al. Interface-tuning of ferroelectricity and quadruple well state in $CuInP_2S_6$ via ferroelectric oxide. *ACS Nano* **17**, 15787–15795 (2023).
[19] Zhou, Z. et al. Unconventional polarization fatigue in van der Waals layered ferroelectric ionic conductor $CuInP_2S_6$. *Nat. Commun*. **14**, 8254 (2023).
[20] Neumayer, S. M. et al. Ionic control over ferroelectricity in 2D layered van der Waals capacitors. *ACS Appl. Mater. Interfaces* **14**, 3018–3026 (2022).
[21] Zhang, D. et al. Anisotropic ion migration and electronic conduction in van der Waals ferroelectric $CuInP_2S_6$. *Nano Lett*. **21**, 995–1002 (2021).
[22] Chen, J. et al. Refreshable memristor via dynamic allocation of ferro-ionic phase for neural reuse. *Nat. Commun.* **16**, 702 (2025).
[23] Lee, J. et al. Free-standing two-dimensional ferro-ionic memristor. *Nat. Commun.* **15**, 5162 (2024).
[24] Zhou, J. et al. 2D Ferroionics: conductive switching mechanisms and transition boundaries in van der Waals layered material $CuInP_2S_6$. *Adv. Mater*. **35**, 2370267 (2023).
[25] Sun, Y. et al. Internal ion transport in ionic 2D $CuInP_2S_6$ enabling multi-state neuromorphic computing with low operation current. *Mater. Today* **66**, 9–16 (2023).
[26] Zhong, Z. et al. Robust threshold-switching behavior assisted by Cu migration in a ferroionic $CuInP_2S_6$ heterostructure. *ACS Nano* **17**, 12563 (2023).
[27] Zhu, H. et al. Highly tunable lateral homojunction formed in two dimensional layered $CuInP_2S_6$ via in-plane ionic migration. *ACS Nano* **17**, 1239 (2023).
[28] Jiang, X. Dual-role ion dynamics in ferroionic $CuInP_2S_6$: revealing the transition from ferroelectric to ionic switching mechanisms. *Nat. Commun.* **15**, 10822 (2024).
[29] Liang, L. et al. Configurable kinetics of polarization switching via ion migration in ferroionic $CuInP_2S_6$. *Nat. Commun.* **16**, 4462 (2025).
[30] Liu, F. et al. Room-temperature ferroelectricity in $CuInP_2S_6$ ultrathin flakes. *Nat. Commun*. **7**, 12357 (2016).
[31] Guo, C. et al. Atomic-level direct imaging for Cu (I) multiple occupations and migration in 2D ferroelectric $CuInP_2S_6$. *Nat. Commun.* **15**, 10152 (2024).
[32] Chen, C. et al. Large-scale domain engineering in two-dimensional ferroelectric $CuInP_2S_6$ via giant flexoelectric effect. *Nano Lett.* **22**, 3275 (2022).
[33] Ming, W. et al. Flexoelectric engineering of van der Waals ferroelectric $CuInP_2S_6$. *Sci. Adv.* **8**, eabq1232 (2022).
[34] Yu, J. et al. Photoinduced Deterministic Polarization Switching in $CuInP_2S_6$ for Multifunctional Optoelectronic Logic Gates. *Nano* Lett. **25**, 3471 (2025).

[35] Zhou, S. et al. Van der Waals layered ferroelectric $CuInP_2S_6$: Physical properties and device applications *Front. Phys.* **16**, 13301 (2021).
[36] Balke, N. et al. Locally Controlled Cu-Ion Transport in Layered Ferroelectric $CuInP_2S_6$. *ACS Appl. Mater. Interfaces* **10**, 27188 (2018).
[37] Maisonneuve, V. et al. Ionic conductivity in ferroic $CuInP_2S_6$ and $CuCrP_2S_6$. *Ferroelectrics* **196**, 257 (1997).
[38] Xu, D. et al. Unconventional out-of-plane domain inversion via in-plane ionic migration in a van der Waals ferroelectric. *J. Mater. Chem. C* **8**, 6966 (2020).
[39] Zhou, S. et al. Anomalous polarization switching and permanent retention in a ferroelectric ionic conductor. *Mater. Horiz.* **7**, 263 (2020).
[40] Zhong, Z. et al. Reconfigurable logic circuits and rectifier based on two-terminal ionic homojunctions. *Device,* **3**, 100712 (2025).
[41] Kalinin, S. et al. Vector piezoresponse force microscopy. *Microsc. Microanal*. **12**, 206 (2006).
[42] Neumayer, S. et al. The concept of negative capacitance in ionically conductive van der Waals ferroelectrics. *Adv. Energy Mater.* 10, 2001726 (2020).
[43] Seleznev, D. et al. Cyclic ferroelectric switching and quantized charge transport in $CuInP_2S_6$. *Phys. Rev. B* **108**, L180101 (2023).
[44] Wu, W. et al. Polarization-modulated rectification at ferroelectric surfaces. *Phys. Rev. Lett.* **104**, 217601 (2010).
[45] Waser, R. Redox-based resistive switching memories-nanoionic mechanisms, prospects, and challenges. *Adv. Mater*. **21**, 2632 (2009).
[46] Yang, Y. el al. Probing memristive switching in nanoionic devices. *Nat. Electron*. **1**, 274 (2018).
[47] Huang, Y. el al. Cu^+ migration and resultant tunable rectification in $CuInP_2S_6$. *ACS Appl. Electron. Mater*. **5**, 5625 (2023).

Acknowledgments

This work is supported by the Ningbo Top Talent Project No. Grant No. 2020-DST-003 (W. Y), Ningbo Yongjiang Talent Introduction Programme No. 2023A-390-G (X. J), the National Natural Science Foundation of China No. 12374080 (X. W), Scientific Research Starting Foundation of Ningbo University of Technology No 2022KQ31 (Z. L).

Author contributions

W. Y. led the conception of the idea and directed the project, assisted by Z. L. and X. J. Z. L. grew the single crystals. M. L., Z. L and X. J. performed the PFM imaging, I-V measurements and data analysis. X. Z. provided the tip-electric field calculation. W. Y. Y., Z. L. and X. J. cowrote the manuscript. Z. P., X. C. D. Z. X. W. contribute to the data discussion.

Competing interests

The authors declare no competing interest.

Supplementary Files

This is a list of supplementary files associated with this preprint. Click to download.

- SupplementaryFile.pdf